International Journal of Hydrogen Energy 73 (2024) 681–694

Contents lists available at ScienceDirect

International Journal of Hydrogen Energy

journal homepage: www.elsevier.com/locate/he

Raman spectroscopy for the determination of hydrogen concentration in liquid organic hydrogen carrier systems

Julius H. Jander [a], Pranay K. Chittem [a], Manuel Kerscher [a], Michael H. Rausch [a], Peter Wasserscheid [b,c,d], Andreas P. Fröba [a,*]

[a] Institute of Advanced Optical Technologies – Thermophysical Properties (AOT-TP), Department of Chemical and Biological Engineering (CBI) and Erlangen Graduate School in Advanced Optical Technologies (SAOT), Friedrich-Alexander-Universität Erlangen-Nürnberg (FAU), Paul-Gordan-Straße 8, 91052 Erlangen, Germany
[b] Institute of Chemical Reaction Engineering (CRT), Department of Chemical and Biological Engineering (CBI), Friedrich-Alexander-Universität Erlangen-Nürnberg (FAU), Egerlandstraße 3, 91058 Erlangen, Germany
[c] Forschungszentrum Jülich GmbH, Helmholtz Institute Erlangen-Nürnberg for Renewable Energy (IEK-11), Cauerstraße 1, 91058 Erlangen, Germany
[d] Forschungszentrum Jülich GmbH, Institute for a Sustainable Hydrogen Economy, Am Brainergy Park 4, 52428 Jülich, Germany

ARTICLE INFO

Handling editor: J. W. Sheffield

Keywords:
Benzyltoluene
Diphenylmethane
Density
Hydrogen solubility
Isochoric-saturation method
Polarization-difference Raman spectroscopy

ABSTRACT

This work reports on the development of a calibration approach of Raman spectroscopy for the determination of the concentration of dissolved hydrogen (H_2) in representative compounds and mixtures of liquid organic hydrogen carrier (LOHC) systems based on diphenylmethane and *ortho*-benzyltoluene (o-BT). Hydrogen solubility data are measured by the isochoric-saturation method at temperatures and pressures up to 473 K and 7 MPa where Raman spectra of the saturated liquid phase are recorded in parallel. By selecting an appropriate frequency range attributed to the LOHC signatures in isotropic spectra, a calibration which is independent of the LOHC system, the degree of hydrogenation of the LOHC samples, and temperature can be found. The transfer of the calibration to another setup is successfully tested up to 523 K and 6 MPa, where H_2 solubilities in the fully hydrogenated o-BT can be determined with an average absolute deviation of 0.009 from theoretically calculated data.

Abbreviations

AAD	average absolute deviation
AARD	average absolute relative deviation
BT	benzyltoluene
DBT	dibenzyltoluene
DoH	degree of hydrogenation
DPM	diphenylmethane
G	gas (phase)
GC-FID	gas chromatography with coupled flame-ionization detection
H	horizontal polarization
H0-DPM	diphenylmethane
H0-o-BT	*ortho*-benzyltoluene
H6-DPM	cyclohexylphenylmethane
H12-o-BT	*ortho*-perhydrobenzyltoluene
H12-DPM	dicyclohexylmethane
ISM	isochoric-saturation method
L	liquid (phase)
LOHC	liquid organic hydrogen carrier
PDRS	polarization-difference Raman spectroscopy
R61-DPM	technical reaction mixture
RS	Raman spectroscopy
SLS	surface light scattering
V	vertical polarization
VLE	vapor-liquid equilibrium

1. Introduction

The utilization of liquid organic hydrogen carriers (LOHCs) is considered to be a viable alternative to conventional methods of hydrogen (H_2) storage at high pressures or by liquification. As LOHCs reversibly bind hydrogen to their molecular structure in a hydrogenation reaction and are liquid at atmospheric pressure over a wide temperature range, they allow for low-loss long-term H_2 storage and

* Corresponding author.
E-mail addresses: julius.jander@fau.de (J.H. Jander), pranay.k.chittem@fau.de (P.K. Chittem), manuel.kerscher@fau.de (M. Kerscher), michael.rausch@fau.de (M.H. Rausch), peter.wasserscheid@fau.de (P. Wasserscheid), andreas.p.froeba@fau.de (A.P. Fröba).

https://doi.org/10.1016/j.ijhydene.2024.05.381
Received 15 April 2024; Received in revised form 23 May 2024; Accepted 24 May 2024
Available online 12 June 2024

Table 1
Specification of used samples.

Substance	CAS number	Source	Molar mass M (g·mol^{-1})	Specified/measured purity or mixture composition
H0-o-BT	713-36-0	self-made	182.26	0.980[a]
H12-o-BT	cis: 54824-04-3 trans: 54823-94-8	self-made	194.36	0.985[a]
H0-DPM	101-81-5	Sigma Aldrich	168.23	0.999[a] $w = 0.999$[b]
H12-DPM	3178-23-2	self-made	180.33	0.998[a]
R61-DPM		self-made	173.37[c]	0.998[a] $x_{\text{H0-DPM}} = 0.346$[d] $x_{\text{H6-DPM}} = 0.460$[d] $x_{\text{H12-DPM}} = 0.194$[d] $DoH = 0.613 \pm 0.002$
Hydrogen	1333-74-0	Air Liquide GmbH	2.016	$y = 0.999999$[b]

[a] Purity determined by GC-FID analysis considering the peak areas of the corresponding regioisomers compared to all peaks after solvent elution obtained in the chromatogram.
[b] Purity as specified by the manufacturer in the certificate of analysis for the used batch.
[c] Effective molar mass of the mixture calculated on the basis of the mixture composition with $M = 174.28$ g·mol^{-1} for the partially hydrogenated H6-DPM (cyclohexylphenylmethane, CAS 4410-75-7).
[d] Mole fraction of main components as measured by GC-FID analysis and used to determine the *DoH*. Impurities are excluded for this.

transport at ambient conditions using the existing fuel infrastructure [1,2]. At the time and location of demand, the stored H_2 can be released from the loaded, hydrogen-rich LOHC compound in a dehydrogenation reaction where the initial hydrogen-lean LOHC molecule is retrieved. Among the LOHC systems based on aromatic hydrocarbon structures as hydrogen-lean compounds, mainly dibenzyltoluene (H0-DBT), benzyltoluene (H0-BT), diphenylmethane (H0-DPM), and toluene with H_2 storage capacities of (6.2, 6.2, 6.7, and 6.2) w-%, respectively, have been in the focus of research and application in the recent years [3–9]. While the LOHC systems based on H0-DBT and H0-BT have been considered to be more technically relevant and are already produced on a larger scale as heat-transfer oils [10], the DPM-based system was utilized as a reference system for systematic studies due to the absence of regioisomerism [11]. Furthermore, H0-DPM was investigated in its eutectic mixture with biphenyl as basis of a tailored LOHC system with a H_2 storage capacity of up to 6.9 w-% [12,13]. For the DPM-based LOHC system, various studies on its thermophysical properties were performed that focused on the influences of, e.g., the degree of hydrogenation [14] and varying concentrations of the co-compound biphenyl [15] or reaction byproducts [15–17] in process-relevant ranges of temperature T. In this context, also the influence of dissolved H_2 on the liquid density [18], the interfacial tension [18,19], and the dynamic viscosity [19] was examined together with the H_2 solubility x_{H2} [18] at pressures p up to 10 MPa. In the reaction processes, x_{H2} plays a crucial role as it influences the reaction rate during hydrogenation as well as the bubble formation during dehydrogenation. In the literature, x_{H2} data at process-relevant p have been reported for the DBT-based LOHC system up to 363 K [20] and for the DPM-based LOHC system up to 702 K [18,21,22] so far.

As LOHC-related processes typically occur out of thermodynamic equilibrium, the measurement of T and p alone cannot be applied for a reliable determination of x_{H2} therein. For the development of methods that allow for corresponding measurements out of vapor-liquid equilibrium (VLE), Raman spectroscopy is a promising candidate as it enables a direct and contactless determination of mixture compositions including liquids with dissolved H_2 in optically accessible systems after appropriate calibration as shown by Ziparo et al. [23] for H_2/water and Kerscher et al. [24] for H_2/methanol.

The present work focuses on the development of a calibration strategy for the determination of the concentration of dissolved H_2 in LOHC systems by Raman spectroscopy. For this purpose, the H_2 solubility x_{H2} in samples representing the LOHC systems based on H0-DPM and the *ortho*-isomer of BT (H0-o-BT) was investigated at T between (323 and 473) K and p up to 7 MPa by the isochoric-saturation method (ISM). In parallel, polarization-difference Raman spectroscopy was applied to the liquid phase in the VLE cell. The deduced calibration has been probed by the evaluation of Raman spectra recorded at T up to 523 K on another setup. Here, the influence of dissolved H_2 on the dynamic viscosity and interfacial tension of LOHCs was studied using surface light scattering [25]. The densities of the saturated liquid phase additionally determined within the ISM setup are compared with compressed liquid-phase density data of the corresponding LOHC samples without dissolved H_2 that were measured at p up to 20 MPa as a reference for identifying the influence of the solute.

2. Experimental

2.1. Materials and sample preparation

Information about the studied substances, their sources, and their purities in terms of mole fraction in the liquid phase, x, or in the gas phase, y, or in form of mass fraction w are provided in Table 1. The used samples of pure LOHC compounds are abbreviated by the indication of the number of bonded hydrogen atoms (H0 or H12) followed by the LOHC system, i.e., DPM or o-BT. For the DPM-based mixture abbreviated with R61-DPM, "R" indicates that the sample stems from a reaction process, while "61" refers to the degree of hydrogenation (*DoH*) in percent, i.e., the share of reversibly bonded hydrogen atoms relative to the maximum uptake capacity of the LOHC system. The Hx-o-BT compounds were synthesized by the hydrodeoxygenation of *ortho*-methylbenzophenone and subsequent catalytic dehydrogenation to obtain *ortho*-benzyltoluene (H0-o-BT) or with subsequent catalytic hydrogenation to receive *ortho*-perhydrobenzyltoluene (H12-o-BT) as described in detail in the Supporting Information of Ref. [25]. The purchased diphenylmethane (H0-DPM) was used as received and hydrogenated to dicyclohexylmethane (H12-DPM) by catalytic hydrogenation as outlined in the Supporting Information of Ref. [14]. The reaction mixture R61-DPM with $DoH = 0.613$ was obtained from a deliberately stopped dehydrogenation reaction of H12-DPM. This mixture also contains the partially hydrogenated cyclohexylphenylmethane (H6-DPM). Gas chromatography with coupled flame-ionization detection (GC-FID) was used to determine the composition and purity of all liquid samples. Prior to their investigation, they were degassed by applying vacuum at $p \approx 2$ Pa for at least 4 h at $T \approx 323$ K. Hydrogen was used as received from the supplier.

2.2. Vibrating-tube densimetry – liquid-phase density

To identify the influence of dissolved H_2 on the liquid density ρ^{L} of the LOHC system at a given p, investigations on the compressed-liquid density ρ^{L}_{comp} without dissolved H_2 were carried out between $T = (293$

Table 2
H_2 solubility in LOHC samples based on o-BT and DPM ($x_{H2,ISM}$) and corresponding vapor phase composition (y_{H2}) as a function of *T*, *p*, and p_{H2} determined by the isochoric saturation method.

T[a]/K	p[b]/ MPa	$\rho^{L}_{sat^*}$[c]/ (kg·m^{-3})	p_{H2}[d]/ MPa	100 × $x_{H2,ISM}$	100 × U ($x_{H2,ISM}$)	100 × y_{H2}[d]	T[a]/K	p[b]/ MPa	$\rho^{L}_{sat^*}$[c]/ (kg·m^{-3})	p_{H2}[d]/ MPa	100 × $x_{H2,ISM}$	100 × U ($x_{H2,ISM}$)	100 × y_{H2}[d]
H0-DPM							**H0-o-BT**						
322.93 ± 0.09	1.065	982.0[e]	1.065	0.26	0.23	100.00	323.46 ± 0.04	1.056	979.2	1.056	0.29	0.17	100.00
322.97 ± 0.07	3.343	982.0[e]	3.343	1.07	0.44	100.00	322.99	3.079	979.6	3.079	1.08	0.33	100.00
322.97 ± 0.07	4.079	982.0[e]	4.079	1.33	0.49	100.00	323.02 ± 0.03	4.104	979.7	4.104	1.41	0.37	100.00
322.96 ± 0.07	6.994	982.0[e]	6.994	2.23	0.63	100.00	323.05	7.005	980.1	7.005	2.56	0.47	100.00
422.92 ± 0.23	1.393	903.1[e]	1.389	0.86	0.22	99.74	423.69 ± 0.21	1.401	902.4	1.399	0.86	0.17	99.83
422.93 ± 0.23	3.290	903.1[e]	3.286	2.09	0.37	99.89	423.18 ± 0.19	3.090	902.8	3.088	1.99	0.28	99.93
422.92 ± 0.23	5.334	903.1[e]	5.331	3.52	0.47	99.93	423.56 ± 0.09	5.421	902.6	5.419	3.55	0.35	99.96
422.88 ± 0.23	7.017	903.1[e]	7.014	4.58	0.55	99.95	423.97 ± 0.10	7.020	903.1	7.018	4.66	0.41	99.97
472.07 ± 0.29	1.563	863.1[e]	1.544	1.22	0.22	98.77	473.79 ± 0.28	1.586	862.3	1.572	1.20	0.17	99.09
472.07 ± 0.26	3.172	863.1[e]	3.153	2.49	0.30	99.40	472.77 ± 0.21	3.069	863.7	3.055	2.41	0.23	99.55
472.06 ± 0.28	5.935	863.1[e]	5.917	4.81	0.46	99.68	473.21 ± 0.13	6.039	863.6	6.025	4.80	0.35	99.77
472.05 ± 0.28	7.051	863.1[e]	7.033	5.60	0.50	99.73	473.74 ± 0.12	7.006	863.4	6.992	5.64	0.37	99.80
H12-DPM							**H12-o-BT**						
323.20	0.996	854.8	0.996	0.67	0.26	100.00	323.29	1.114	858.0	1.114	0.52	0.29	100.00
323.18	3.107	854.8	3.107	2.34	0.48	100.00	323.30	3.022	858.2	3.022	1.84	0.54	100.00
323.23	4.050	854.8	4.050	3.00	0.54	100.00	323.26	4.035	858.3	4.035	2.45	0.60	100.00
323.23	7.012	854.8	7.012	5.24	0.67	100.00	323.19 ± 0.03	7.013	858.5	7.013	5.00	0.82	100.00
423.25 ± 0.06	1.297	783.8	1.291	1.42	0.25	99.55	423.20 ± 0.03	1.446	788.5	1.443	1.39	0.29	99.77
423.31 ± 0.06	3.114	783.7	3.108	3.47	0.41	99.82	422.87 ± 0.03	3.044	788.9	3.041	3.17	0.46	99.89
423.26 ± 0.07	5.248	783.7	5.242	5.84	0.51	99.89	422.82	5.153	788.9	5.150	5.51	0.57	99.94
423.29 ± 0.06	7.017	783.7	7.012	7.71	0.58	99.92	423.11	7.027	789.1	7.024	7.76	0.72	99.96
473.34 ± 0.07	1.460	747.9[f]	1.430	1.87	0.25	97.90	472.71 ± 0.05	1.605	752.7	1.589	1.90	0.28	99.02
473.29 ± 0.07	3.102	747.9[f]	3.072	3.96	0.34	99.03	472.54	2.986	752.4	2.971	3.69	0.38	99.48
473.23 ± 0.08	5.833	747.9[f]	5.804	7.43	0.49	99.50	472.71	5.618	751.9	5.603	7.25	0.55	99.73
473.20 ± 0.08	7.022	748.0	6.994	8.72	0.53	99.59	472.72 ± 0.03	7.088	753.3	7.074	8.92	0.65	99.79
R61-DPM													
323.11	1.025	898.2	1.025	0.39	0.20	100.00	422.94 ± 0.07	5.140	824.5	5.136	4.50	0.39	99.91
323.10	3.030	898.4	3.030	1.62	0.37	100.00	422.92 ± 0.07	6.863	825.0	6.859	6.14	0.45	99.94
323.10	3.964	898.5	3.964	2.09	0.41	100.00	472.95 ± 0.11	1.511	785.6	1.487	1.44	0.19	98.40
323.10	6.971	898.8	6.971	3.97	0.51	100.00	472.91 ± 0.10	3.086	785.8	3.062	2.98	0.26	99.22
422.91 ± 0.07	1.342	824.3	1.338	1.05	0.19	99.66	472.93 ± 0.10	5.672	785.8	5.649	5.91	0.38	99.59
422.88 ± 0.07	3.094	824.6	3.090	2.57	0.31	99.86	472.93 ± 0.11	7.029	786.3	7.006	7.07	0.40	99.67

[a] The reported *T* correspond to the average of the readings of the two *T* probes located close to the vapor and liquid phase in the VLE cell. If the reading of a probe deviated more from this average than its calibrated uncertainty, this difference is indicated as interval behind the value. Otherwise, $U(T) = 0.02$ K holds.

[b] For all samples except for H0- and H12-DPM, the reported *p* is the average of the readings for the two *p* transducers with calibrated uncertainties of $U(p) = (5$ and 15) kPa connected to the gas phase of the VLE cell and in the circulation loop. As the values always agreed within uncertainty, $U(p) = 5$ kPa for the listed *p*. The same uncertainty holds for the data for H0- and H12-DPM because only the transducer connected to the VLE cell was used.

[c] Liquid density close to saturation with H_2 obtained by slight adjustments with respect to T from the values reported in Table 8 or Ref. [18] as described in the Appendix. If not indicated otherwise by footnote d or e, $U_r(\rho^L_{sat^*}) = 0.2\%$.

[d] Taking into consideration also deviations from ideal assumptions, the relative uncertainties of the partial pressure of hydrogen and of the derived vapor-phase composition at the lowest p was estimated to be smaller than $U_r(p_{H2}) \approx U_r(y_{H2}) = (0.1, 0.3, \text{and } 0.5)\%$ at $T = (323, 423, \text{and } 473)$ K, respectively. With increasing p, $U_r(p_{H2})$ and $U_r(y_{H2})$ are closer to, but always larger than $U_r(p) = 0.05\%$.

[e] $U_r(\rho^L_{sat^*}) = 0.3\%$.

[f] $U_r(\rho^L_{sat^*}) = 0.4\%$.

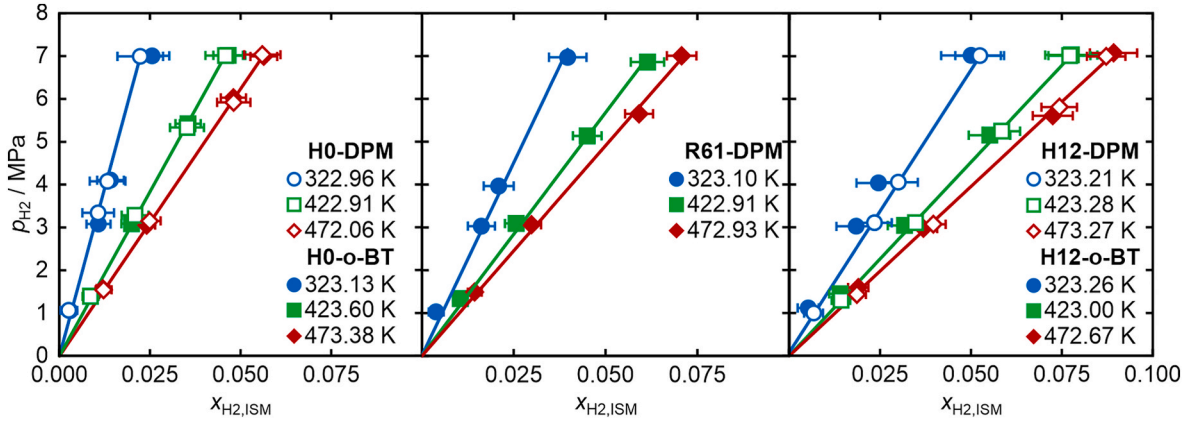

Fig. 1. Solubility of H_2 in H0-o-BT or H0-DPM (left), R61-DPM (middle), and H12-o-BT or H12-DPM (right) up to $T \approx 473$ K and $p = 7$ MPa determined by the ISM, $x_{H2,ISM}$, expressed as the partial pressure of H_2, p_{H2}, as a function of the H_2 mole fraction in the saturated liquid phase. The solid lines correspond to linear fits constrained to coincide with the axis intersect which are exemplarily shown for the DPM-based LOHC system representatives. (For interpretation of the references to color in this figure legend, the reader is referred to the Web version of this article.)

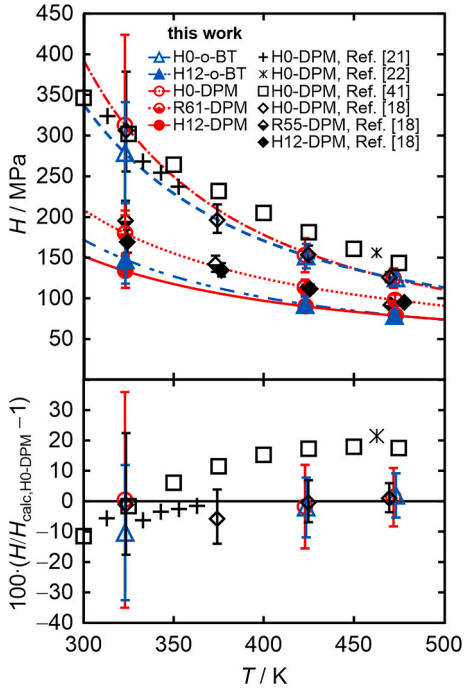

Fig. 2. Upper part: Henry's law constants H from Table 3 for representatives of the LOHC systems based on DPM (circles) and o-BT (triangles) calculated from the x_{H2} data given in Table 2. The lines correspond to the T-dependent correlation of the data by Eq. (4) with the parameters given in Table 4. In addition, data for H0-DPM from Qin et al. [21], Simnick et al. [22], Cukor and Prausnitz [41], as well as our previously published data [18] are included. Lower part: Relative deviation of available H data for H0-DPM or H0-BT from H_{calc} for H0-DPM by Eq. (4) with the parameters obtained in this work. (For interpretation of the references to color in this figure legend, the reader is referred to the Web version of this article.)

Table 3
Henry's law constants H approximated by the slope of the linear fit of p_{H2} as a function of x_{H2} with the physical constraint that $p_{H2} = 0$ MPa at $x_{H2} = 0$ calculated from the results obtained by ISM given in Table 2.

T[a]/K	H/MPa	$100 \cdot U_r(H)$[b]	T[a]/K	H/MPa	$100 \cdot U_r(H)$[b]
H0-DPM			**H0-o-BT**		
322.96 ± 0.03	312	35	323.13 ± 0.14	279	22
422.91 ± 0.03	153	14	423.60 ± 0.42	152	9.9
472.06	125	10	473.38 ± 0.61	125.0	7.3
H12-DPM			**H12-o-BT**		
323.21 ± 0.03	134	16	323.26 ± 0.07	147	20
423.28 ± 0.03	90.4	8.6	423.00 ± 0.18	92.1	10
473.27 ± 0.07	79.1	6.7	472.67 ± 0.13	78.8	7.9
R61-DPM					
323.10	180	16			
422.91 ± 0.03	113.6	8.4			
472.93	98.2	6.4			

[a] Average T of the state points on the isotherm. The interval corresponds to the maximum deviation of a single measurement point from the average T reported. Otherwise $U(T) = 0.02$ K holds.

[b] Mean relative difference between H and the two H values obtained by applying the same fitting procedure after increasing or decreasing the x_{H2} values by $U(x_{H2})$ for a given sample and T.

and 473) K at $p = (1, 3, 7, 10, \text{and } 20)$ MPa for H0-o-BT, H12-o-BT, and R61-DPM as for these substances, corresponding data were not available. These measurements were performed with the vibrating-tube densimeter (DMA 4200 M, Anton Paar) that was also used within the ISM setup to measure the density of the liquid phase of the LOHC samples containing dissolved H_2. The T control system integrated in the

Table 4
Parameters for Eq. (4) from the correlation of the H values given in Table 3 for the LOHC samples investigated within this work between $T \approx$ (323 and 473) K and p up to 7 MPa.

Sample	H_0	H_1	100·AARD[a]
H0-DPM	2.82	944	1.2
R61-DPM	3.27	621	0.36
H12-DPM	3.23	53[a]	0.023
H0-o-BT	3.09	820	0.30
H12-o-BT	3.02	638	0.10

[a] Average absolute relative deviation (AARD) of the data from the fit.

densimeter is associated with an expanded (coverage factor $k = 2$) uncertainty of $U(T) = 30$ mK. For the pure LOHC samples, p was adjusted with a connected screw press and measured with a pressure transducer (PA-33X, Keller) with a specified expanded ($k = 2$) uncertainty of $U(p) = 15$ kPa, while details on the determination of p related to measurements on the ISM setup are given in the next section. The density values were obtained from the directly measured oscillation periods and T as well as the time-averaged p using the calibration detailed in Ref. [18] and following the approach proposed by May et al. [26]. In brief, the physically-based device parameters were determined based on reference measurements at T between (293 and 473) K under vacuum as well as for water and toluene at p up to 40 MPa, where expanded ($k = 2$) relative uncertainties of 0.1% were deduced.

2.3. Isochoric-saturation method (ISM) – solubility

The hydrogen solubility x_{H2} was investigated for H0- and H12-o-BT, H0- and H12-DPM as well as for R61-DPM using the isochoric-saturation method (ISM). The experimental setup including the evaluation procedure has been described in detail in Ref. [18] and was also used in further works, e.g., in the context of x_{H2} measurements with the solvent methanol [24] where Raman spectroscopy has been employed as well. In the following, a brief description of the details relevant for the present study is given.

The main part of the setup consists of a sample cell where a VLE is established and of a liquid circulation line in which the aforementioned densimeter is integrated. During the saturation process with the injected gas, the liquid is continuously circulated through the densimeter to ensure therein the same liquid-phase composition as in the VLE cell. Since the liquid density of H0- and H12-DPM with dissolved H_2 was already studied in Ref. [18], the circulation part of the setup could be omitted for the investigations of these LOHC samples and only the VLE cell was employed.

The T regulation for the VLE cell and the circulation pump was achieved by resistance heating using Pt-100Ω resistance probes calibrated with an expanded ($k = 2$) uncertainty of $U(T) = 20$ mK and located close to the outer walls of the elements to be heated. For the individual state points, the reported T corresponds to the average of the readings from two further Pt-100Ω probes with the same uncertainty located close to the center of the VLE cell wall adjacent to the gas and the liquid phase. The pressure was measured by two p transducers (PAA-33X and PA-33X, Keller) connected to the VLE cell and the circulation line with expanded ($k = 2$) uncertainties of $U(p) =$ (5 and 15) kPa. In all experiments in which the circulation line was used, their recorded values agreed within 5.1 kPa.

Between (90 and 140) g of liquid LOHC sample was filled stepwise into the previously helium-purged VLE cell *via* a syringe, which was weighed before and afterwards on a balance with a digit precision of 0.1 mg and an estimated expanded ($k = 2$) uncertainty of 1 mg. Thereafter, the cell was evacuated and H_2 was injected from a pressure vessel. For the simultaneous investigations of ρ^L for H0- and H12-o-BT as well as for R61-DPM with dissolved H_2, the outlet valve to the circulation line was opened in the next step such that the liquid filled the evacuated circulation volume.

The amount of H_2 added to the total volume of the VLE was calculated using the calibrated volume of the gas-dosing branch including the pressure vessel and the gas density of H_2 determined *via* the reference correlation from Ref. [27] implemented in the REFPROP 10.0 database [28]. For that, p and T were measured before and after the injection by a pressure transducer (PA-33X, Keller, $U(p) = 15$ kPa, $k = 2$) and a calibrated Pt-100Ω probe with $U(T) = 20$ mK ($k = 2$) placed inside the pressure vessel.

At each state point, the system was left for equilibration for at least 2 h. During that time, the liquid phase in the VLE cell was continuously stirred until the recorded p and, if used, the oscillation period of the densimeter reached stable values. After stopping the stirrer and the pump as well as a brief compensation time for the slight instabilities induced hereby, x_{H2} was evaluated iteratively from a closed set of equations. This evaluation relies on mass conservation of the added LOHC and H_2 aiming at the determination of the mass distribution of both components in the liquid and gas phase. To this end, the isochoric conditions of the VLE system are utilized together with the measured T, p, and ρ^L with dissolved H_2, described by $\rho^L_{sat^*}$ in the following. Here, the asterisk in the subscript indicates a state very close to saturation due to slight T differences between the VLE cell and the densimeter.

For the evaluation of x_{H2}, the remaining mass of H_2 in the gas phase is calculated from the gas-phase volume V^G and the gas density of H_2 [27] at the measured T and the partial pressure p_{H2} before subtracting the result from the total mass of H_2 injected into the VLE. As the vapor pressure $p_{vap,LOHC}$ of the LOHC species is low, p_{H2} is calculated as the difference between the measured total system p and $p_{vap,LOHC}$ considering Dalton's and Raoult's laws. The vapor pressure of the LOHC is obtained from Refs. [10,29] for H0-o-BT and H12-o-BT as well as from Refs. [30–32] for H0- and H12-DPM. For R61-DPM, $p_{vap,LOHC}$ is estimated based on Raoult's law from the known LOHC mixture composition, where $p_{vap,LOHC}$ of H6-DPM is assumed to be the average of the vapor pressures of H0- and H12-DPM.

The volume of the gas phase (V^G) is obtained from the known total volume of the VLE system and the liquid-phase volume V^L. The latter can be accessed from the total mass of the liquid phase m^L and information on the H_2-saturated liquid-phase density $\rho^L_{sat^*}$ measured in-line for H0- and H12-o-BT as well as for R61-DPM in the present study or taken from our previous study [18] for H0- and H12-DPM. A detailed description of the calculation of $\rho^L_{sat^*}$ from the measured and published [18] data accounting for small differences between T in the VLE cell and in the densimeter is provided in the Appendix. Variations in p do not need to be considered since in VLE with H_2 at a given T, any p dependencies in $\rho^L_{sat^*}$ of the studied LOHC samples could neither be resolved in Ref. [18] nor in the present study, cf. section 3.3.

In the first step of the iteration, m^L is set equal to the total mass of LOHC filled into the system. After each iteration loop, m^L is recalculated as the sum of the masses of LOHC and H_2 in the liquid phase considering their individual mass balances. The iteration is continued until the relative mass change of H_2 in the liquid phase between two loops is smaller than 1×10^{-12}. In each iteration step, the LOHC mass in the gas phase is estimated on the basis of $p_{vap,LOHC}$ and the ideal-gas law. The total amount of H_2 present in the VLE was corrected slightly whenever an unavoidable loss of H_2 through the gaskets at larger p and T occurred. To quantify this loss, the time-dependent change of the partial density of H_2 in the gas phase owing to the small linear changes in p at quasi-steady-state conditions, i.e., after the equilibration to reach a new state point, was combined with V^G of the subsequent evaluated state point and the elapsed time. During heating or cooling periods, the corresponding mass loss rates of the neighboring state points were averaged. The relative expanded uncertainty of the individually performed mass corrections is estimated to be 10%. The absolute expanded uncertainty of the finally obtained H_2 solubility data $U(x_{H2})$ was calculated by error propagation in quadrature considering the individual uncertainties of all input quantities in the described set of equations.

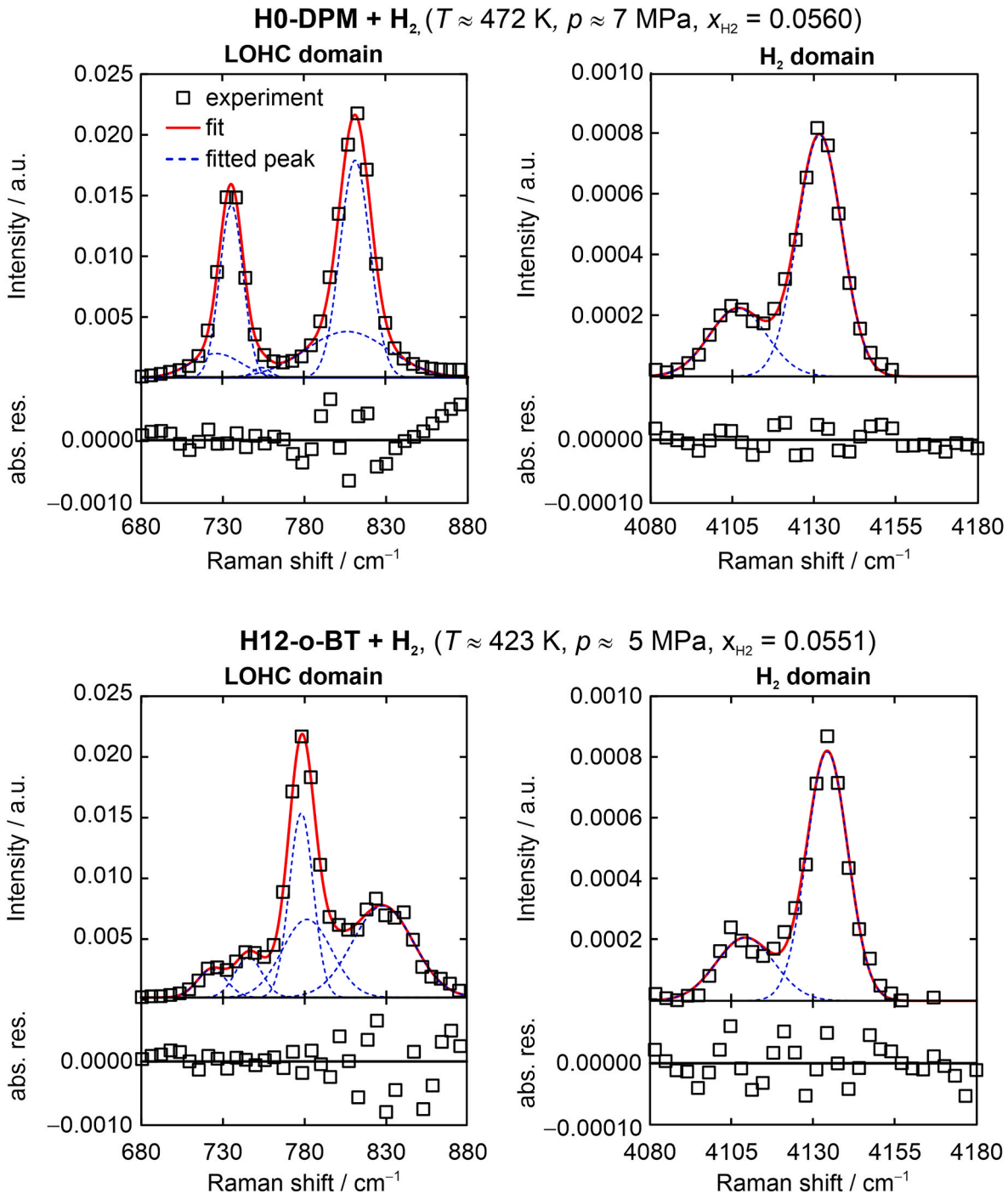

Fig. 3. Examples for the peak fit of the baseline-corrected I_{iso} Raman spectra of H0-DPM (top) or H12-o-BT (bottom) with dissolved H_2 at $T \approx$ (472 or 423) K and $p =$ (7.051 or 5.158) MPa at a comparable $x_{H2} =$ (0.0551 or 0.0560) normalized to $I_{LOHC} = 1$. The blue dotted lines correspond to the individual Gaussian peaks which, in sum (red solid line), describe the spectra data (square symbols) in the given frequency range. In the lower part of the segmented plots, the absolute residuals of the experimental data from the fit are shown. (For interpretation of the references to color in this figure legend, the reader is referred to the Web version of this article.)

2.4. Raman spectroscopy (RS) – mixture composition

In parallel to the ISM measurements, in total 16 Raman spectra were recorded from the H_2-saturated liquid phase of the LOHC samples at each state point. For this, the Raman spectroscopy (RS) setup described in detail in Refs. [24,33] with a laser of slightly different wavelength (Cobolt Samba, $\lambda_0 = 532$ nm) was used. Vertical (V) and horizontal (H) incident laser polarization was adjusted by a $\lambda/2$ waveplate while a fixed V polarization of the detected light entering the spectrometer (QEPro, Ocean Optics) in backscattering direction was maintained. This resulted in 8 polarized and 8 depolarized intensity spectra (I_{VV} and I_{HV}) for each sample and state point. The incident laser power was typically adjusted to 200 mW, but was sometimes lowered over the period of investigations to (100, 50, or 20) mW when strong absorption and/or fluorescence in the sample was observed. To test the transferability of the desired calibration, further polarization-dependent Raman spectra were recorded in 90°-scattering configuration during investigations of the interfacial tension and dynamic viscosity of H12-o-BT with dissolved H_2 by surface light scattering (SLS) [25] on the setup described in Ref. [24] which is referred to as SLS setup in the following. Here, the applied incident laser

Table 5
H_2 solubility determined by Raman spectroscopy $x_{H2,RS}$ *via* Eq. (3) using K_{all} given in Table 6 and I_r.[a]

T/K	p/MPa	I_r	$U(I_r)$	$100 \cdot x_{H2,RS}$	$100 \cdot U(x_{H2,RS})$	$100 \cdot (x_{H2,RS} - x_{H2,ref})$[b]
H0-DPM						
322.93 ± 0.09	1.065	680	130	0.49	0.16	0.23
322.97 ± 0.07	3.343	235	17	1.40	0.39	0.33
322.97 ± 0.07	4.079	188.6	7.1	1.74	0.47	0.41
322.96 ± 0.07	6.994	100.6	2.3	3.21	0.86	0.98
422.92 ± 0.23	1.393	313.9	6.0	1.05	0.29	0.19
422.93 ± 0.23	3.290	138.8	2.3	2.35	0.63	0.26
422.92 ± 0.23	5.334	84.24	0.55	3.8	1.0	0.28
422.88 ± 0.23	7.017	64.52	0.27	4.9	1.3	0.32
472.07 ± 0.29	1.563	237.6	2.1	1.38	0.38	0.16
472.07 ± 0.26	3.172	122.93	0.81	2.64	0.71	0.15
472.06 ± 0.28	5.935	65.73	0.54	4.8	1.3	−0.01
472.05 ± 0.28	7.051	54.17	0.45	5.8	1.5	0.20
R61-DPM						
323.11	1.025	700	420	0.47	0.31	0.08
323.10	3.030	117.9	4.2	2.75	0.75	1.13
323.10	3.964	143.5	8.7	2.27	0.62	0.18
323.10	6.971	61.6	1.7	5.1	1.3	1.13
422.91 ± 0.07	1.342	271	21	1.22	0.34	0.17
422.88 ± 0.07	3.094	93.9	1.6	3.43	0.92	0.86
422.94 ± 0.07	5.140	64.2	2.8	4.9	1.3	0.40
422.92 ± 0.07	6.863	46.6	2.3	6.7	1.8	0.56
472.95 ± 0.11	1.511	225	46	1.46	0.49	0.02
472.91 ± 0.10	3.086	90.4	8.4	3.6	1.0	0.58
472.93 ± 0.10	5.672	49.2	1.4	6.3	1.7	0.39
472.93 ± 0.11	7.029	38.77	0.58	7.9	2.0	0.83
H12-DPM						
323.20	0.996	465	59	0.71	0.21	0.04
323.18	3.107	149.8	7.1	2.18	0.59	−0.16
323.23	4.050	96.7	9.2	3.33	0.94	0.33
323.23	7.012	59.3	2.1	5.3	1.4	0.06
423.25 ± 0.06	1.297	255	13	1.29	0.36	−0.13
423.31 ± 0.06	3.114	104.3	1.1	3.10	0.83	−0.37
423.26 ± 0.07	5.248	55.3	0.72	5.7	1.5	−0.14
423.29 ± 0.06	7.017	40.79	0.58	7.6	1.9	−0.11
473.34 ± 0.07	1.460	216.3	9.9	1.52	0.42	−0.34
473.29 ± 0.07	3.102	95.79	0.65	3.36	0.89	−0.60
473.23 ± 0.08	5.833	42.95	0.59	7.2	1.8	−0.23
473.20 ± 0.08	7.022	37.22	0.37	8.2	2.1	−0.52
H0-o-BT						
323.46 ± 0.04	1.056	Inf[c]	Inf[c]	–	–	–
322.99	3.079	73	18	4.4	1.5	3.32
323.02 ± 0.03	4.104	500	1100	0.7	1.5	−0.71
323.05	7.005	83	35	3.9	1.9	1.34
423.69 ± 0.21	1.401	216	55	1.52	0.56	0.66
423.18 ± 0.19	3.090	85.16	0.95	3.77	1.00	1.78
423.56 ± 0.09	5.421	75	14	4.3	1.4	0.75
423.97 ± 0.10	7.020	59.7	1.7	5.3	1.4	0.64
473.79 ± 0.28	1.586	Inf[c]	Inf[c]	–	–	–
472.77 ± 0.21	3.069	370	430	0.9	1.1	−1.51
473.21 ± 0.13	6.039	62.5	2.5	5.1	1.3	0.30
473.74 ± 0.12	7.006	56.1	4.0	5.6	1.5	−0.04
H12-o-BT (ISM setup)						
323.29	1.114	343	11	0.96	0.26	0.44
323.30	3.022	125.8	9.7	2.58	0.72	0.74
323.26	4.035	101.99	0.67	3.16	0.84	0.71
323.19 ± 0.03	7.013	60.59	0.36	5.2	1.4	0.20
423.20 ± 0.03	1.446	193.6	2.1	1.69	0.46	0.30
422.87 ± 0.03	3.044	100.27	0.60	3.22	0.86	0.05
422.82	5.153	57.04	0.58	5.5	1.4	−0.01
423.11	7.027	41.72	0.49	7.4	1.9	−0.36
472.71 ± 0.05	1.605	167.9	2.7	1.95	0.53	0.05
472.54	2.986	89.05	0.66	3.61	0.96	−0.08
472.71	5.618	44.87	0.26	6.9	1.8	−0.35
472.72 ± 0.03	7.088	37.43	0.31	8.2	2.1	−0.72
H12-o-BT (SLS setup)						
323.14	2.974	136	11	2.39	0.67	0.37
323.14	6.006 ± 0.03	75	24	4.3	1.7	0.23
373.09 ± 0.07	5.997 ± 0.04	44.57	0.42	7.0	1.8	1.71
423.17	2.988	74.985	0.067	4.3	1.1	1.07
423.13	5.997	41.9	1.4	7.4	1.9	0.92
473.10 ± 0.07	5.907	37.3	1.6	8.2	2.1	0.73
523.05 ± 0.10	2.996	62.6	9.0	5.1	1.5	0.87
523.01 ± 0.13	5.968	31.90	0.26	9.5	2.4	0.98

[a] For the systems investigated on the ISM setup, $U(T) = 0.02$ K and $U(p) = 5$ kPa or is given behind the value (cf. footnote a in Table 2). The uncertainties on the SLS setup are deduced from the calibrated expanded uncertainties of the T probes and p transducer, i.e., $U(T) = 0.03$ K and $U(p) = 5$ kPa plus the standard deviation of the recorded values. Thus, the uncertainties [b]re $U(T) = 0.04$ K and $U(p) = 20$ kPa or stated behind the value. $U(I_r)$ and $U(x_{H2,RS})$ are given in the table.

[b] $x_{H2,ref}$ calculated for the measurements on the SLS setup from H_{calc} and the recorded p and T where H_{calc} was obtained *via* Eq. (4) using the parameters in Table 4. Otherwise, $x_{H2,ref}$ corresponds to $x_{H2,ISM}$ from Table 2.

[c] Division by $I_{H2} = 0$ in Eq. (2). Excluded from the determination of K values and further calculations.

powers were between (40 and 100) mW, where the laser wavelength is the same as on the ISM setup.

As demonstrated in Refs. [34,35], fluorescence can be sufficiently attenuated or even completely suppressed by polarization-difference Raman spectroscopy (PDRS) *via* subtracting two spectra obtained at different polarization states. For the present optical arrangement on both setups, the isotropic spectrum analyzed for the determination of solubility can be calculated on the basis of the recorded I_{VV} and I_{HV}

Table 6
Calibration factors K determined by fitting I_r with respect to $x_{H2,ISM}$ from Table 2 by Eq. (3) for individual LOHC samples and T, $K(T)$, for an individual LOHC sample at all T, K_{LOHC}, and for all LOHC samples at all T, K_{all}.

T/K[a]	$K(T)$ or K_{LOHC} or K_{all}	$U(K)$[b]
H0-DPM		
322.96 ± 0.03	0.429	0.030
422.91 ± 0.03	0.3241	0.0062
472.06	0.309	0.013
all T	*0.316*	*0.016*[c]
R61-DPM		
323.10	0.399	0.066
422.91 ± 0.03	0.344	0.053
472.93	0.336	0.014
all T	*0.341*	*0.044*[c]
H12-DPM		
323.21 ± 0.03	0.306	0.021
423.28 ± 0.03	0.290	0.015
473.27 ± 0.07	0.280	0.021
all T	*0.284*	*0.019*[c]
^{H}0-o-BT		
323.13 ± 0.03	0.72[d]	0.68
423.60 ± 0.42	0.42	0.19
473.24 ± 0.47	0.309[d]	0.048
all T	*0.37*[d]	*0.31*[c]
H12-o-BT		
323.26	0.327	0.051
423.00	0.293	0.020
472.67	0.280	0.013
all T	*0.288*	*0.028*[c]
all	**0.300**	**0.083**[e]

[a] Average T of the state points investigated on the ISM setup from Table 2 or 5. The interval behind the value indicates the maximum deviation of the individual values at an isotherm from the reported average. The interval is omitted for deviations smaller than the uncertainty of the T measurement. In this case $U(T)$ = 0.02 K.
[b] Expanded ($k = 2$) uncertainty calculated from the residuals of the data to the fit.
[c] Average of $U(K)$ of the three T investigated.
[d] The data points at the lowest p at $T \approx$ (323 and 473) K where I_r approaches infinity are not considered.
[e] Average of $U(K)$ for all systems at the individual T.

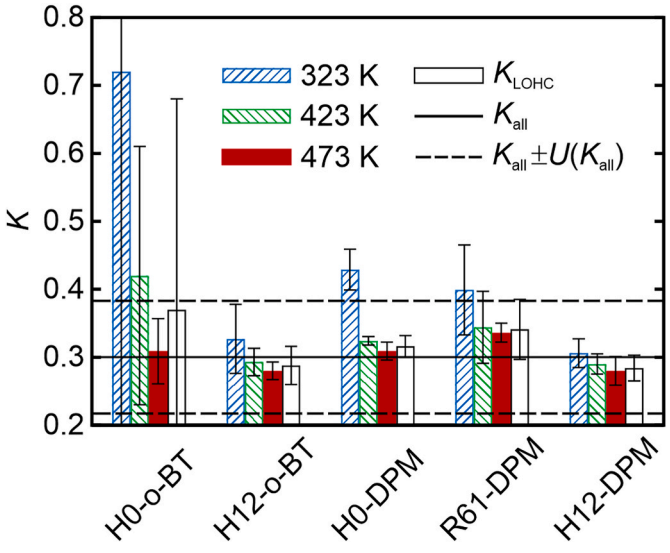

Fig. 4. K factors from Table 6 determined by the correlation of $x_{H2,ISM}$ from Table 2 with I_r given in Table 5 by Eq. (3) for samples from the LOHC systems based on o-BT and DPM. (For interpretation of the references to color in this figure legend, the reader is referred to the Web version of this article.)

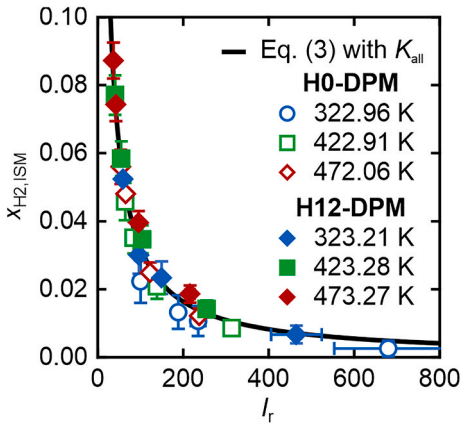

Fig. 5. Calibration curve (line) calculated by Eq. (3) using K_{all} from Table 6 together with $x_{H2,ISM}$ and I_r data for H0- and H12-DPM (open and closed symbols). (For interpretation of the references to color in this figure legend, the reader is referred to the Web version of this article.)

spectra according to Refs. [36–38] by

$$I_{iso}(\nu) = \frac{1}{64} \times \sum_{i=1}^{8} \sum_{j=1}^{8} \left[I_{VV}^{(i)}(\nu) - \frac{4}{3} I_{HV}^{(j)}(\nu) \right]. \quad (1)$$

The resulting I_{iso} was then baseline-corrected by selecting points in the spectra where no Raman signatures are present by the MATLAB function of Ref. [39].

As the relative intensities of Raman bands originating from corresponding species in a mixture are directly proportional to the species fraction, RS can be employed to determine mixture compositions. However, it needs to be calibrated beforehand using Raman spectra from samples with known composition. In this work, this is enabled by the simultaneous acquisition of Raman spectra from the saturated liquid phase studied in the ISM setup regarding the concentration of H_2 in the LOHC sample in VLE, x_{H2}. The intensity ratio

$$I_r = \frac{I_{LOHC}}{I_{H2}} \quad (2)$$

was calculated from selected peak areas in the Raman spectra attributed to the LOHC, I_{LOHC}, or H_2, I_{H2}. As proposed in Ref. [40], a calibration factor K can be obtained from the correlation of selected sets of I_r and x_{H2} data *via*

$$x_{H2} = \frac{1}{1 + I_r K}. \quad (3)$$

Details on an appropriate selection of suitable Raman bands for a reliable determination of mixture composition by RS and the associated uncertainties are given in section 3.2.

3. Results and discussion

3.1. Hydrogen solubility

The results for the H_2 solubility in the DPM- and o-BT-based LOHC samples determined by the ISM, $x_{H2,ISM}$, up to $p = 7$ MPa and $T \approx 473$ K are summarized in Table 2 and are depicted in Fig. 1 as a function of the partial pressure of H_2, p_{H2}, for the three isotherms investigated. In the figure, the data for the fully dehydrogenated and fully hydrogenated samples are shown in the left and right diagrams, while the diagram in the center displays results for the partially hydrogenated technical mixture with $DoH = 0.613$.

For all samples investigated, x_{H2} shows a linear relationship with p_{H2}, which is highlighted in Fig. 1 for the DPM-based samples by the solid linear fit lines fixed in the axis intersect. The solubility of H_2

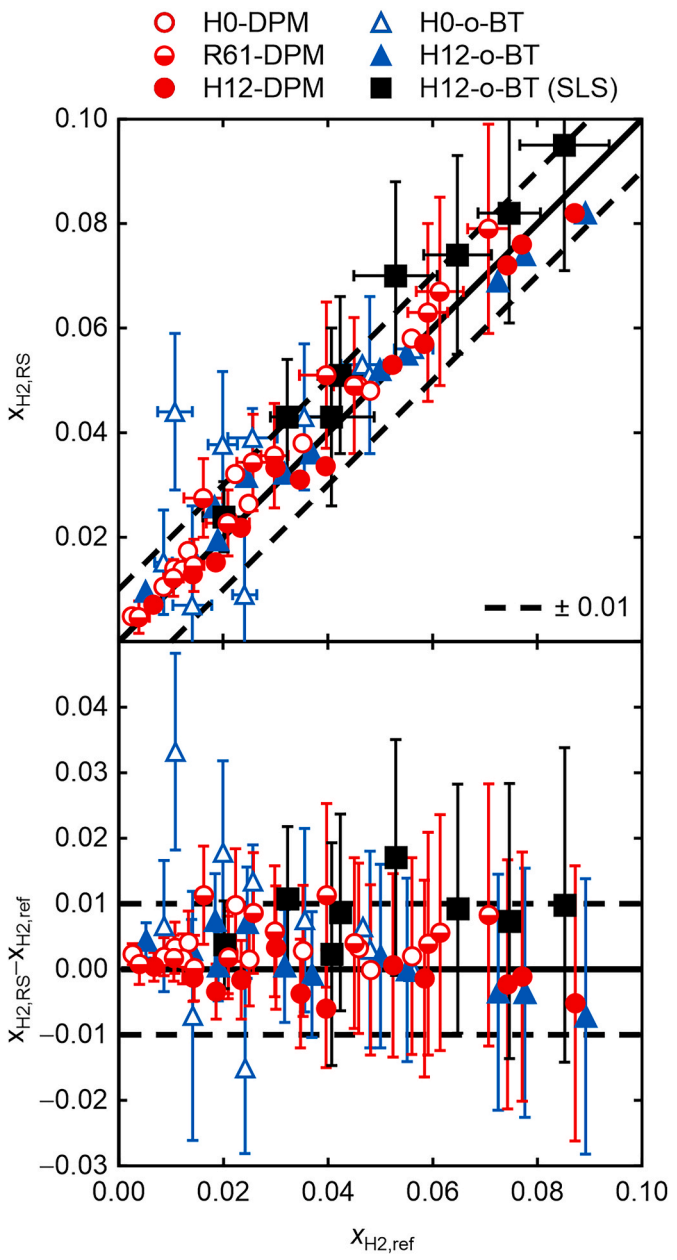

Fig. 6. H_2 solubility $x_{H2,RS}$ in samples from the DPM- and o-BT-based LOHC systems (red circles and blue triangles) calculated by Eq. (3) with K_{all} and I_r obtained from Raman spectroscopy (upper part) and its deviation from $x_{H2,ref}$ (lower part) as a function of $x_{H2,ref}$ according to Table 5. $x_{H2,ref}$ corresponds either to $x_{H2,ISM}$ from Table 2 or was calculated for H12-o-BT investigated on the SLS setup (black squares) at the measured p and T from H_{calc} *via* Eq. (4). Dashed lines indicate a deviation of ±0.01 in terms of mole fraction. (For interpretation of the references to color in this figure legend, the reader is referred to the Web version of this article.)

increases with increasing p_{H2} and T, which can also be seen in the works of Qin et al. [21], Simnick et al. [22] or Cukor and Prausnitz [41] who investigated x_{H2} in H0-DPM at p and T up to 6.2 MPa between (313 and 363) K, up to 25 MPa between (463 and 702) K, or at 0.1 MPa between (298 and 473) K, respectively.

Considering the experimental uncertainties, any differences in the x_{H2} behavior among the fully dehydrogenated or the fully hydrogenated DPM- and o-BT-based compounds cannot be resolved. In this connection, it should be noted that the relatively large uncertainties $U_r(x_{H2})$ predominantly observable at $T = 323$ K and the lowest p can be attributed to the challenge in detecting H_2 mole fractions of around 0.005, which corresponds to H_2 mass fractions of around 0.00003. At $T \approx$ (323 and 473) K, the x_{H2} data for the fully hydrogenated LOHC compounds are by factors of about 2 and 1.6 larger than for the dehydrogenated species at the same p. Similar observations have also been reported for the cyclic hydrocarbon LOHC systems based on dibenzyltoluene/perhydrodibenzyltoluene [20] and toluene/methylcyclohexane [8,20].

To allow for a more direct comparison between the different LOHC system representatives, the results are summarized in Fig. 2 as a function of T in the form of Henry's law constants H for the individual isotherms and samples. H is approximated by the slope of the linear fit of p_{H2} as a function of x_{H2} with the physical constraint that $p_{H2} = 0$ MPa at $x_{H2} = 0$. The calculated values of H can be found in Table 3. The corresponding expanded ($k = 2$) uncertainty $U(H)$ shown as error bars in Fig. 2 and given together with H in Table 3 was calculated as the mean difference between H and the two H values obtained by applying the same fitting procedure after increasing or decreasing the x_{H2} values by $U(x_{H2})$ for a given sample and T. Thus, it can be interpreted as a worst-case uncertainty. The lines in Fig. 2 correspond to the correlation of the individual values of H for a given sample with respect to T as proposed in Ref. [42] by a truncated power series in the form of

$$\ln[H_{calc}(T) / \text{MPa}] = H_0 + H_1 \cdot (\text{K} / T), \tag{4}$$

where the resulting parameters H_0 and H_1 can be found in Table 4.

In addition, data for H0-DPM from Qin et al. [21], Cukor and Prausnitz [41] and Simnick et al. [22] who calculated Henry's law constants between $T =$ (313 and 363) K, $T =$ (300 and 475) K, and $T \approx$ (463 and 702) K from solubility measurements up to $p \approx 6.2$ MPa, at $p \approx$ 1 atm, and up to $p \approx 25$ MPa, respectively, are included in Fig. 2. In Ref. [21], the authors employed the ISM, whereas Cukor and Prausnitz [41] used a static experimental method based on an apparatus designed by Dymond and Hildebrand [43]. In Ref. [22], x_{H2} was determined from a flow apparatus where the saturated liquid was sampled and then analyzed at ambient conditions by measuring the volume of desorbed H_2 and weighing the residual liquid solvent.

The largest deviation of the data from Qin et al. [21] from H_{calc} is −6.3% at 333 K, which reduces with increasing T to −1.5% at 363 K. For Cukor and Prausnitz [41], the deviation from H_{calc} is about −1.6% at T = 325 K, which is close to the lowest T studied here, and increases to about +18% at larger T. From Simnick et al. [22], the single data point located within the investigated T range of this work is about 21% larger than H_{calc}. These discrepancies occurring predominately at elevated T might be related to the differences in the employed measurement techniques, the investigated system pressures, and/or the different approaches in data evaluation.

In the upper part of Fig. 2, further H values from our recent publication are included for H0-DPM, H12-DPM, and a partially hydrogenated reaction mixture with $DoH \approx 0.55$, R55-DPM. These data were measured with the same ISM setup as described here, but without applying RS. The figure shows that for the technical mixtures R55-DPM [18] and R61-DPM with $DoH \approx$ (0.55 and 0.61), the H values align accordingly between H0- and H12-DPM reported in this work. Furthermore, the series for H0-o-BT, H0-DPM from this work and Ref. [18] as well as those for H12-o-BT and H12-DPM from this work coincide. Considering these behaviors, one may conclude that the previously published data for H12-DPM [18] being in good agreement with those of the reaction mixtures are erroneous. A corresponding suspicion has already been stated in this publication [18], yet only with respect to the data at $T \approx 323$ K. In the light of the present data, it rather seems that the complete measurement series for H12-DPM in Ref. [18] was affected by an unknown effect and should not be further considered.

3.2. *Determination of H_2 concentration by Raman spectroscopy*

The foremost challenge of the calibration of RS for the determination of the concentration of dissolved H_2 in liquid LOHC samples was the

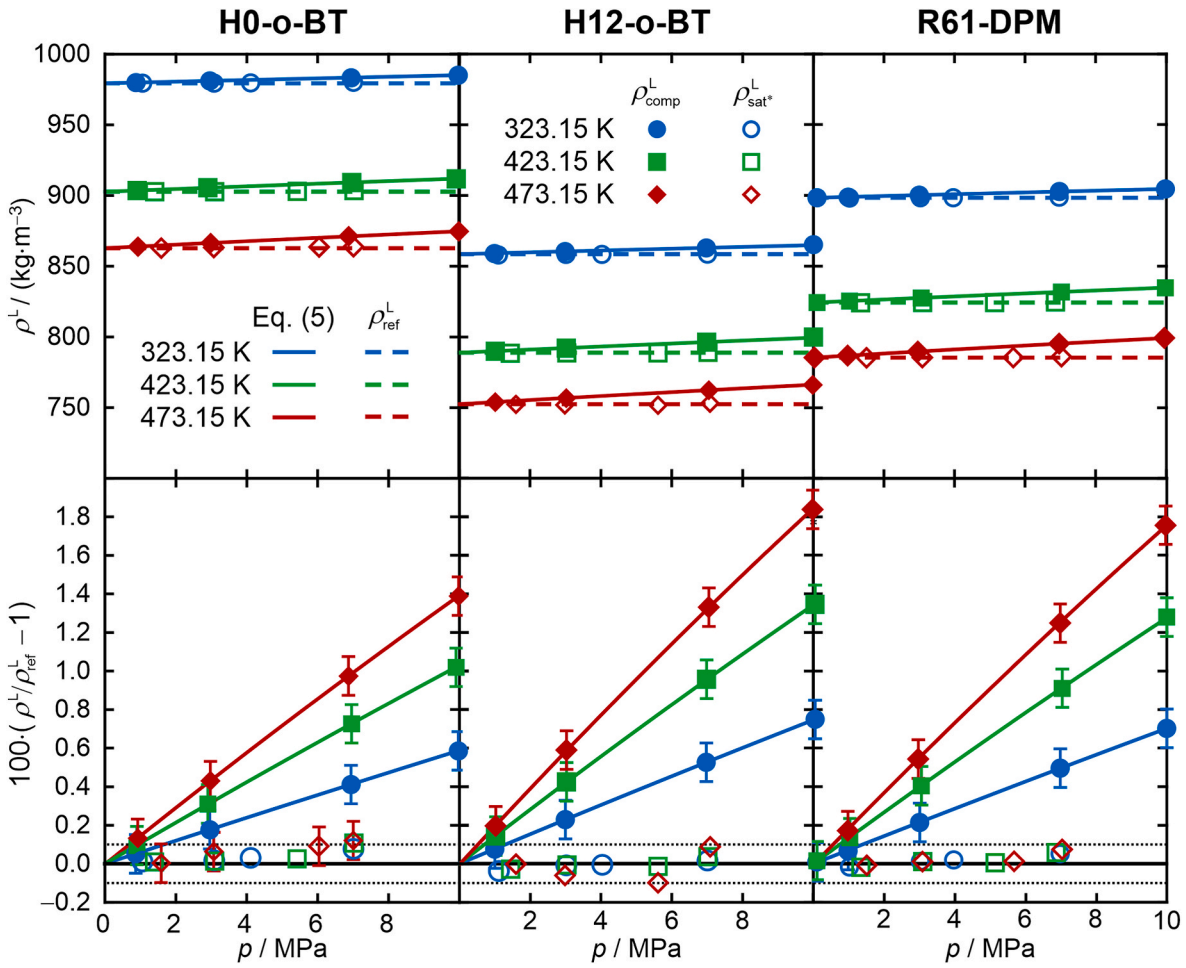

Fig. 7. Upper part: Compressed-liquid density ρ^{L}_{comp} (filled symbols) of pure H0-o-BT (left), H12-o-BT (middle), and R61-DPM (right) as well as their liquid-phase density close to saturation with H_2 ρ^{L}_{sat*} (open symbols) as a function of system p. In addition, the p-dependent fit of the ρ^{L}_{comp} data by Eq. (5) using the parameters given in Table 9 are included by solid lines. The dashed lines correspond to the result of Eq. (5), ρ^{L}_{ref}, evaluated at p_{vap} of the LOHC sample at the corresponding T. Lower part: Relative deviations of ρ^{L}_{comp} and H_2-saturated liquid density of the LOHC samples from ρ^{L}_{ref}. Dotted black lines indicate $U_r(\rho^{L}_{ref})$. (For interpretation of the references to color in this figure legend, the reader is referred to the Web version of this article.)

identification of a suitable Raman-shift range especially for the LOHC molecules of interest that yields consistent relations between I_r and x_{H2} at all relevant T. This way, a universal calibration constant K could be applied to all corresponding technical mixtures and states. For I_{H2}, the H_2 signature located around $\nu \approx 4130$ cm^{-1} is an obvious choice that was maintained throughout all calibration attempts. For I_{LOHC}, first evaluations of the Raman spectra considered the CH-stretching region located in the Raman shift range between $\nu \approx$ (2800 and 3250) cm^{-1} because of the strong Raman intensities present in all considered LOHC molecules independent of their hydrogenation state. This approach, however, revealed a strong dependency of K on the *DoH* of the LOHC system, where K of the dehydrogenated and hydrogenated species of the same LOHC system differed by a factor of about 2. The evaluation of several further approaches showed that the region of ν between (680 and 880) cm^{-1} is more suitable for the purpose of this work. Within this ν range, the sum of the peak areas of the dehydrogenated and hydrogenated species for both the o-BT- and the DPM-based systems relative to the area of the H_2 signature remains similar for the studied *DoH* and T at a comparable x_{H2} as shown in Fig. 3. There, exemplary results from the peak-fit routine of the background-corrected spectra are depicted for H0-DPM (upper part) and H12-o-BT (lower part) at a similar x_{H2}.

The intensity areas of the LOHC (left) or H_2 (right), I_{LOHC} or I_{H2}, were obtained by summing up the individual peak areas of the 6 or 2 Gaussian peaks fitted in the corresponding range from $\nu =$ (680 to 880) cm^{-1} or (4080 to 4180) cm^{-1}. The corresponding absolute uncertainties in I_{LOHC} and I_{H2} were determined from the residuals of the fit to the individual spectrum data and the respective ν intervals. To improve the comparability in Fig. 3, the spectra for the two samples have been normalized to result in $I_{LOHC} = 1$. Like this, it can be seen that the area covered by the H_2-related Raman shift region is very similar for comparable concentrations of H_2 dissolved in H0-DPM and H12-o-BT. The intensity ratios I_r calculated by Eq. (2) from the corresponding peak areas of H_2 and the LOHC samples in the isotropic spectra can be found in Table 5. Using $x_{H2,ISM}$ from Table 2 measured at the same state points, the calibration factors K summarized in Table 6 and depicted in Fig. 4 were determined from the correlation of different sets of (I_r, $x_{H2,ISM}$) data points *via* Eq. (3) weighted by the sum of the inverse of the relative uncertainties $U_r(I_r)$ and $U_r(x_{H2,ISM})$. In Fig. 4, K calculated for each sample and T, $K(T)$, is indicated by bars dashed upwards for $T = 323$ K, bars dashed downwards for $T = 423$ K, and filled bars for $T = 473$ K. The results from the fit of the data of each individual sample independent of T, K_{LOHC}, are represented by open bars, and K_{all} given as solid line corresponds to the fit of all available I_r and $x_{H2,ISM}$ data irrespective of the sample and T. The expanded ($k = 2$) absolute fit uncertainty of $K(T)$ was determined from the statistical quality of the weighted fit. For the sample-specific and T-independent K_{LOHC}, $U(K_{LOHC})$ is the arithmetic mean of the contributing $U(K)$ at the three T. The uncertainty $U(K_{all})$ is obtained from the average of all T-dependent $U(K)$. In Fig. 4, the uncertainties are

Table 7
Liquid density of H0- and H12-o-BT as well as R61-DPM without dissolved H_2 measured as a function of T and p.[a]

T/K	p/MPa	ρ^{L}_{comp}/(kg·m^{-3})	T/K	p/MPa	ρ^{L}_{comp}/(kg·m^{-3})
H0-o-BT			**H12-o-BT**		
298.15	0.905	998.64	298.15	1.017	876.25
298.15	2.913	999.69	298.15	2.984	877.39
298.15	6.899	1001.74	298.15	6.970	879.65
298.15	9.926	1003.28	298.15	10.007	881.34
298.15	19.901	1008.17	298.15	19.962	886.65
323.15	0.872	979.80	323.15	0.999	859.04
323.15	2.954	981.03	323.15	2.997	860.35
323.15	6.940	983.32	323.15	6.979	862.90
323.15	9.963	985.03	323.15	10.045	864.81
323.15	19.981	990.48	323.15	20.021	870.73
373.15	0.910	942.15	373.15	1.014	824.74
373.15	2.866	943.72	373.15	3.021	826.43
373.15	6.949	946.58	373.15	6.971	829.66
373.15	9.934	948.69	373.15	10.021	832.06
373.15	19.889	955.41	373.15	19.993	839.46
398.15	0.926	923.02	398.15	0.998	807.45
398.15	2.930	924.73	398.15	3.010	809.47
398.15	6.935	928.02	398.15	7.014	813.13
398.15	9.923	930.41	398.15	9.983	815.77
398.15	19.959	937.99	398.15	20.073	824.14
423.15	0.904	903.58	423.15	1.029	789.92
423.14	2.901	905.53	423.15	3.029	792.13
423.15	6.955	909.28	423.15	6.987	796.33
423.15	9.905	911.93	423.15	10.046	799.40
423.15	19.971	920.43	423.15	20.048	808.71
448.15	0.927	883.99	448.15	0.988	771.97
448.15	2.968	886.22	448.15	3.005	774.54
448.15	6.949	890.42	448.15	6.955	779.31
448.15	9.926	893.43	448.15	10.022	782.83
448.15	19.961	902.92	448.15	20.004	793.22
473.15	0.926	863.96	473.15	1.025	753.87
473.15	2.977	866.53	473.15	3.029	756.82
473.15	6.868	871.22	473.15	7.051	762.40
473.15	9.972	874.79	473.15	9.984	766.22
473.15	19.910	885.31	473.15	20.019	777.97
R61-DPM					
298.15	0.1[b]	916.66	398.15	7.183	849.85
298.15	1.057	917.12	398.15	10.117	852.46
298.15	3.003	918.24	398.15	20.050	860.72
298.15	6.982	920.50	423.14	0.1[b]	824.45
298.15	10.006	922.18	423.15	1.028	825.43
298.15	20.055	927.55	423.15	3.055	827.65
323.14	0.1[b]	898.38	423.15	7.031	831.82
323.15	0.985	898.90	423.15	9.978	834.86
323.15	3.005	900.22	423.15	19.989	844.15
323.15	6.975	902.75	448.14	0.1[b]	805.26
323.15	9.978	904.60	448.15	0.998	806.28
323.15	20.006	910.56	448.15	2.966	808.75
348.15	0.1[b]	880.11	448.15	7.031	813.62
373.15	0.1[b]	861.75	448.15	10.053	817.07
373.15	1.067	862.52	448.15	20.024	827.49
373.15	3.049	864.17	473.15	0.1[b]	785.66
373.15	7.032	867.41	473.15	0.973	786.85
373.15	9.966	869.72	473.15	2.965	789.76
373.15	20.089	877.23	473.15	6.970	795.30
398.14	0.1[b]	843.30	473.15	9.944	799.29
398.15	1.031	844.08	473.15	19.919	811.06
398.15	2.986	845.98			

[a] The expanded ($k = 2$) uncertainties are $U(T) = 0.03$ K, $U(p) = 15$ kPa, and $U_r(\rho^{L}_{comp}) = 0.1\%$.
[b] Measured without pressure transducer against atmospheric p.

indicated as dashed lines for K_{all} or by error bars for the other K values.

Fig. 4 shows that both dehydrogenated LOHC compounds at $T = 323$ K exhibit the largest deviation with respect to K_{all} as well as to K_{LOHC}, which is outside the combined uncertainties for H0-DPM at $T \approx 323$ K or coupled with large uncertainty for H0-o-BT. For all other T and samples, however, the $K(T)$ values typically agree with K_{all} within uncertainties. The relatively large discrepancy at $T \approx 323$ K is linked to the small x_{H2} at low T and *DoH*, which is more than three times lower for the fully dehydrogenated compounds than for the fully hydrogenated LOHCs at the largest T. This situation is illustrated in Fig. 5 for the example of the DPM-based system by a comparison of the corresponding $x_{H2,ISM}$ and I_r data.

Here, it becomes obvious that especially for H0-DPM at $T = 323$ K, the available data points do not allow for an accurate fitting of the calibration line at small I_r. This situation is further deteriorated for H0-o-BT, where the quality of the spectra was compromised by pronounced fluorescence which probably originated from byproducts or residuals from the synthesis from methylbenzophenone by hydrodeoxygenation and the subsequent dehydrogenation over a long time period at elevated T. Here, the H_2 signature is hardly distinguishable from the noise of the baseline, predominately at low x_{H2}. This leads to large scattering of the I_r values, which is also reflected in the large error bars of the four K values obtained for H0-o-BT. The good agreement of K at 473 K for H0-o-BT with the corresponding values for the other samples, however, shows that the selected ν regimes should also be suitable for this LOHC representative.

With exception of the discussed outliers at $T = 323$ K, which is rather far below the process-relevant T range, the $K(T)$ and K_{LOHC} for the individual samples generally agree within their uncertainties, meaning that K can be considered to be T-independent. As also the individual T-averaged K_{LOHC} match within combined uncertainties, it is straightforward to deduce a universal calibration factor for the studied range of LOHC representatives and T. As the obtained K_{all} agrees with all K_{LOHC} values, this calibration factor can be used for the determination of the concentration of dissolved H_2 in both studied LOHC systems independent of T and the *DoH*. Similar to this, T-independent Raman calibration factors have also been found, e.g., in our previous studies on mixtures of methanol with dissolved H_2 [24] as well as on mixtures of H0- and H12-DPM aiming at a measurement of the *DoH* of this system by Raman spectroscopy [44].

In a next step, K_{all} and I_r determined from the I_{iso} spectra obtained on the ISM setup as well as on the SLS setup at VLE were evaluated *via* Eq. (3) to obtain $x_{H2,RS}$. The results are included in Table 5 together with their absolute deviations from $x_{H2,ref}$ which corresponds to $x_{H2,ISM}$ from Table 2 for the measurements performed on the ISM setup. For the transfer study to the SLS setup with H12-o-BT, where the influence of dissolved H_2 on the viscosity and interfacial tension of this LOHC compound was studied [25], $x_{H2,ref}$ was calculated from the measured p and T *via* H_{calc} according to Eq. (4) using the coefficients given in Table 4. The expanded ($k = 2$) uncertainty $U(x_{H2,RS})$ was determined by error propagation in quadrature considering the individual $U(I_r)$ values and $U(K_{all})$ relevant for Eq. (3). The obtained results are depicted in Fig. 6 in form of a parity plot of $x_{H2,RS}$ and $x_{H2,ref}$ (upper part) as well as of the absolute deviation $x_{H2,RS} - x_{H2,ref}$ as a function of $x_{H2,ref}$ (lower part).

Most $x_{H2,RS}$ data shown in Fig. 6 deviate by less than 0.01 from $x_{H2,ref}$. The largest scattering can be observed for H0-o-BT, which is related to the low signal-to-noise ratios in the Raman spectra originating from large fluorescence backgrounds in combination with a generally low x_{H2}, as discussed in context with the determination of K. H0- and R61-DPM exhibit a slight positive bias towards larger values of $x_{H2,RS}$, which are on average about 0.0041 larger than $x_{H2,ISM}$. In total, the average absolute deviation (AAD) of $x_{H2,RS}$ from $x_{H2,ISM}$ for the DPM-based LOHC samples is 0.0036 while the average absolute uncertainty of $x_{H2,RS}$ is 0.0096. For the o-BT-based LOHC samples studied on the ISM setup, the AAD is 0.0092 for H0-o-BT, 0.0034 for H12-o-BT, as well as 0.0068 for both in combination, where the average absolute uncertainty is 0.012. For H12-o-BT examined on the SLS setup, the datapoint at $T \approx 373$ K and $p \approx 6$ MPa exhibits the largest deviation of about +0.017 from $x_{H2,ref}$. Nevertheless, both values agree within their combined uncertainties. Including this outlier, the AAD of $x_{H2,RS}$ determined on the SLS setup from $x_{H2,ref}$ is 0.0086, which gives a first positive indication regarding the transferability of the calibration for the determination of the H_2 concentration using RS to other setups or applications and even

Table 8
Liquid density of H0- and H12-o-BT as well as R61-DPM with dissolved H_2 measured as a function of T and p as well as x_{H2} from Table 2 determined in parallel by the ISM.[a]

T/K	p/MPa	$100 \cdot x_{H2}$	$\rho^{L}_{sat^*}$/(kg·m^{-3})	T/K	p/MPa	$100 \cdot x_{H2}$	$\rho^{L}_{sat^*}$/(kg·m^{-3})
H0-o-BT				**H12-o-BT**			
323.15	1.056	0.29	979.42	323.15	1.114	0.52	858.06
323.15	3.079	1.08	979.48	323.15	3.022	1.84	858.32
323.15	4.104	1.41	979.61	323.15	4.035	2.45	858.34
323.15	7.005	2.56	980.06	323.15	7.013	5.00	858.53
423.15	1.401	0.86	902.81	423.15	1.446	1.39	788.56
423.15	3.090	1.99	902.85	423.15	3.044	3.17	788.73
423.15	5.421	3.55	902.96	423.15	5.153	5.51	788.68
423.15	7.020	4.66	903.70	423.15	7.027	7.76	789.07
473.15	1.586	1.20	862.84	473.15	1.605	1.90	752.37
473.15	3.069	2.41	863.36	473.15	2.986	3.69	751.93
473.15	6.039	4.80	863.60	473.15	5.618	7.25	751.64
473.15	7.006	5.64	863.86	473.15	7.088	8.92	753.05
R61-DPM							
323.15	1.025	0.39	898.14	423.15	5.140	4.50	824.36
323.15	3.030	1.62	898.41	423.15	6.863	6.14	824.80
323.15	3.964	2.09	898.47	473.15	1.511	1.44	785.44
323.15	6.971	3.97	898.76	473.15	3.086	2.98	785.58
423.15	1.342	1.05	824.16	473.15	5.672	5.91	785.60
423.15	3.094	2.57	824.41	473.15	7.029	7.07	786.08

[a] The expanded ($k = 2$) uncertainties are $U(T) = 0.03$ K, $U(p) = 5$ kPa, and $U_r(\rho^{L}_{sat^*}) = 0.1\%$. $U(x_{H2})$

Table 9
Coefficients of Eq. (5) to calculate the compressed-liquid density ρ^{L}_{calc} of H0-o-BT, H-12-o-BT, and R61-DPM as a function of p at different T determined from ρ^{L}_{comp} data up to $p \approx 20$ MPa.

T/K	ρ^{L}_0/(kg·m^{-3})	ρ^{L}_1/(kg·m^{-3}·MPa^{-1})	ρ^{L}_2/(kg·m^{-3}·MPa^{-2})	100·AARD[a]
H0-o-BT				
323.15	979.29	0.59254	−0.0016224	0.00036
423.15	902.72	0.97396	−0.0043652	0.0011
473.15	862.79	1.2775	−0.0073510	0.00048
H12-o-BT				
323.15	858.38	0.66381	−0.0023468	0.00013
423.15	788.78	1.1238	−0.0064723	0.0012
473.15	752.36	1.5003	−0.011042	0.0016
R61-DPM				
323.15	898.29	0.65167	−0.0019088	0.0012
423.15	824.31	1.1150	−0.0061136	0.0023
473.15	785.46	1.4873	−0.010121	0.0039

[a] AARD of the measured ρ^{L}_{comp} from the fit.

different scattering geometries. The average of the absolute uncertainties of $x_{H2,RS}$ obtained from the Raman spectra acquired on the SLS setup is 0.016 and, thus, clearly larger than the AAD.

Overall, $x_{H2,ref}$ can be represented by $x_{H2,RS}$ for all DPM- and o-BT based LOHC samples with an AAD of 0.0053 and an average absolute uncertainty of 0.011 over the full T and p range up to $T \approx 473$ K and $p \approx 7$ MPa on the ISM setup and up to $T \approx 523$ K and $p \approx 6$ MPa on the SLS setup using the single calibration constant K_{all}.

3.3. Liquid density – compressed liquids and close to saturation with H_2

The liquid densities of H0- and H12-o-BT as well as of R61-DPM determined within this work are shown in Fig. 7. The corresponding data for the compressed liquid without H_2, ρ^{L}_{comp}, and close to saturation with H_2, $\rho^{L}_{sat^*}$, can be found in Table 7 and Table 8. For R61-DPM, the additionally measured data at ambient p are also included therein. To ensure legibility, the data representation in Fig. 7 is limited to the p range and isotherms where $\rho^{L}_{sat^*}$ and $x_{H2,ISM}$ were investigated. The solid lines correspond to the correlation of the ρ^{L}_{comp} data for the individual isotherms measured up to $p \approx 20$ MPa by

$$\rho^{L}_{calc}(p) = \rho^{L}_0 + \rho^{L}_1 p + \rho^{L}_2 p^2, \quad (5)$$

where the fit parameters are provided in Table 9. The dashed lines indicate the liquid density without dissolved H_2, ρ^{L}_{ref}, at p_{vap} calculated by Eq. (5).

The upper part of Fig. 7 shows that ρ^{L} generally decreases with increasing T. With respect to the pure liquids, ρ^{L}_{comp} increases linearly with p. It exhibits a larger compressibility at higher T and larger DoH, indicated by a more pronounced p-dependent increase, which is also associated with lower ρ^{L}_{comp} at ambient p for the mentioned cases.

In contrast to ρ^{L}_{comp}, no significant change of $\rho^{L}_{sat^*}$ with increasing system p can be observed for all three LOHC samples. Here, the dissolved H_2 appears to counteract the volume compression of the LOHC by the applied p while introducing a neglectable increase in the total liquid mass. Except for H0-o-BT at the largest p at $T =$ (423 and 473) K, the relative deviations from ρ^{L}_{ref} are smaller than the uncertainty $U_r(\rho^{L}) = 0.1\%$, but also for these exceptions, agreement within combined uncertainties is given. Such virtually p-independent density behavior under the influence of dissolved H_2 at saturation conditions was also found for LOHC samples based on DPM in a previous study [18].

4. Conclusion

The present work focuses on the development of a calibration approach for Raman spectroscopy (RS) for the determination of the concentration of dissolved hydrogen (H_2) in bicyclic liquid organic hydrogen carrier (LOHC) systems. For this, the H_2 solubility (x_{H2}) was determined in representative samples for the LOHC systems based on diphenylmethane (DPM) and *ortho*-benzyltoluene (o-BT) with a degree of hydrogenation (*DoH*) between 0 and 1 at temperatures T and pressures p up to 473 K and 7 MPa by the isochoric-saturation method (ISM). In parallel to these solubility measurements, the liquid density of H0- and H12-o-BT as well as R61-DPM with dissolved H_2 has been investigated in-line with the equilibrium cell. Here, the liquid density was found to be p-independent up to about 7 MPa, which indicates a mutual compensation of the effects of dissolved H_2 and the pressure exerted by the H_2 atmosphere. The additionally measured compressed-liquid density of the pure LOHC samples in a similar p range increased by about (1 and 1.3)% for H0-o-BT and H12-o-BT at $T \approx 473$ K.

x_{H2} shows a linear relationship with p and increases with increasing T for all studied samples. For the two different fully dehydrogenated and hydrogenated LOHC species, x_{H2} agrees within uncertainties and is between (2 and 1.6) times larger for the hydrogenated compounds at T between (323 and 473) K. For a partially hydrogenated DPM-based technical mixture with a *DoH* of 0.613, the H_2 solubility is roughly between those of H0- and H12-DPM, with a tendency towards H12-DPM. Henry's law constants were approximated and correlated as a function of T to allow for the calculation of H_2 solubility at other state points.

Based on Raman spectra of the saturated liquid phase recorded during the solubility measurements, the targeted calibration of RS for the determination of H_2 concentration was achieved by selecting the frequency range from (680 to 880) cm^{-1} in the isotropic Raman spectra attributed to the signatures of the LOHC species. The resulting calibration factor was found to be independent of T, LOHC system, and *DoH*. The calibration was tested on another experimental setup, where an average uncertainty of 0.016 was achieved for x_{H2} measured by RS. Its average absolute deviation (AAD) from the results obtained *via* the correlation of Henry's law constants was 0.0086. Taking into consideration the deviations of the x_{H2} data obtained by RS on the ISM setup from the directly measured x_{H2} data as well, the AAD is 0.0053. In total, x_{H2} could be determined on both setups with an average uncertainty of 0.011 over the complete range of p and T for all five LOHC samples studied.

Funding sources

This work was funded by the Bavarian Ministry of Economic Affairs, Regional Development and Energy as well as by the German Research Foundation (Deutsche Forschungsgemeinschaft, DFG) under Grant No. FR 1709/27-1.

CRediT authorship contribution statement

Julius H. Jander: Writing – original draft, Investigation, Conceptualization. **Pranay K. Chittem:** Writing – review & editing, Investigation. **Manuel Kerscher:** Writing – review & editing, Investigation. **Michael H. Rausch:** Writing – review & editing. **Peter Wasserscheid:** Writing – review & editing. **Andreas P. Fröba:** Writing – review & editing, Supervision, Conceptualization.

Declaration of competing interest

The authors declare there are no competing interests.

Acknowledgements

The authors gratefully acknowledge funding of the Erlangen Graduate School in Advanced Optical Technologies (SAOT) by the Bavarian State Ministry for Science and Art.

Appendix

For H0- and H12-o-BT as well as for R61-DPM, where $\rho^{L}_{sat^*}$ was accessed in-line with the VLE cell, the directly measured values were slightly shifted by the T dependency obtained from the T-dependent second-order polynomial correlation of the pure-substance ρ^{L} at $p = 0.1$ MPa to match the slightly different T in the VLE cell. The corresponding parameters used for H0- and H12-o-BT were taken from Ref. [25], whereas for R61-DPM, the T-dependent fit equation is

$$\frac{\rho^{L}_{calc}(T)}{(kg \cdot m^{-3})} = 1113.60 - 0.607162 \cdot (T/K) - 0.000180931 \cdot (T/K)^2. \quad (6)$$

Since only slight adjustments related to T were performed, the resulting $U_r(\rho^{L}_{sat^*})$ is estimated to be 0.2% for the systems where $\rho^{L}_{sat^*}$ was measured during the ISM experiments. For H0- and H12-DPM, ρ^{L}_{calc} of the pure substances was calculated directly with T measured for the VLE cell and the parameters determined by Kerscher et al. [45]. Here, the associated relative expanded uncertainty is estimated to be 0.3%.

References

[1] Preuster P, Papp C, Wasserscheid P. Liquid organic hydrogen carriers (LOHCs): toward a hydrogen-free hydrogen Economy. Acc Chem Res 2017;50:74–85. https://doi.org/10.1021/acs.accounts.6b00474.

[2] Modisha PM, Ouma CNM, Garidzirai R, Wasserscheid P, Bessarabov D. The prospect of hydrogen storage using liquid organic hydrogen carriers. Energy Fuel 2019;33:2778–96. https://doi.org/10.1021/acs.energyfuels.9b00296.

[3] Teichmann D, Arlt W, Wasserscheid P, Freymann R. A future energy supply based on liquid organic hydrogen carriers (LOHC). Energy Environ Sci 2011;4:2767. https://doi.org/10.1039/c1ee01454d.

[4] Niermann M, Drünert S, Kaltschmitt M, Bonhoff K. Liquid organic hydrogen carriers (LOHCs) – techno-economic analysis of LOHCs in a defined process chain. Energy Environ Sci 2019;12:290–307. https://doi.org/10.1039/c8ee02700e.

[5] Markiewicz M, Zhang YQ, Bösmann A, Brückner N, Thöming J, Wasserscheid P, Stolte S. Environmental and health impact assessment of liquid organic hydrogen carrier (LOHC) systems – challenges and preliminary results. Energy Environ Sci 2015;8:1035–45. https://doi.org/10.1039/C4EE03528C.

[6] Geburtig D, Preuster P, Bösmann A, Müller K, Wasserscheid P. Chemical utilization of hydrogen from fluctuating energy sources – catalytic transfer hydrogenation from charged liquid organic hydrogen carrier systems. Int J Hydrogen Energy 2016;41:1010–7. https://doi.org/10.1016/j.ijhydene.2015.10.013.

[7] Modisha P, Bessarabov D. Stress tolerance assessment of dibenzyltoluene-based liquid organic hydrogen carriers. Sustain Energy Fuels 2020;4:4662–70. https://doi.org/10.1039/d0se00625d.

[8] Tsuji T, Shinya Y, Hiaki T, Itoh N. Hydrogen solubility in a chemical hydrogen storage medium, aromatic hydrocarbon, cyclic hydrocarbon, and their mixture for fuel cell systems. Fluid Phase Equil 2005;228–229:499–503. https://doi.org/10.1016/j.fluid.2004.07.013.

[9] Ojelade OA, Zaman SF. Dehydrogenation and hydrogenation cycle of methylcyclohexane–toluene system for liquid phase hydrogen storage: thermodynamic reaction equilibrium investigation. Arabian J Sci Eng 2022;47:6223–32. https://doi.org/10.1007/s13369-021-06162-w.

[10] Müller K, Stark K, Emel'yanenko VN, Varfolomeev MA, Zaitsau DH, Shoifet E, Schick C, Verevkin SP, Arlt W. Liquid organic hydrogen carriers: thermophysical and thermochemical studies of benzyl- and dibenzyl-toluene derivatives. Ind Eng Chem Res 2015;54:7967–76. https://doi.org/10.1021/acs.iecr.5b01840.

[11] Amende M, Gleichweit C, Xu T, Höfert O, Koch M, Wasserscheid P, Steinrück HP, Papp C, Libuda J. Dicyclohexylmethane as a liquid organic hydrogen carrier: a model study on the dehydrogenation mechanism over Pd(111). Catal Lett 2016; 146:851–60. https://doi.org/10.1007/s10562-016-1711-z.
[12] Kwak Y, Moon S, Ahn C, Kim A-R, Park Y, Kim Y, Sohn H, Jeong H, Nam SW, Yoon CW, Jo YS. Effect of the support properties in dehydrogenation of biphenyl-based eutectic mixture as liquid organic hydrogen carrier (LOHC) over Pt/Al_2O_3 catalysts. Fuel 2021;284:119285. https://doi.org/10.1016/j.fuel.2020.119285.
[13] Han DJ, Jo YS, Shin BS, Jang M, Kang JW, Han JH, Nam SW, Yoon CW. A novel eutectic mixture of biphenyl and diphenylmethane as a potential liquid organic hydrogen carrier: catalytic hydrogenation. Energy Technol 2019;7:113–21. https://doi.org/10.1002/ente.201700694.
[14] Schmidt PS, Kerscher M, Klein T, Jander JH, Berger Bioucas FE, Rüde T, Li S, Stadelmaier M, Hanyon S, Fathalla RR, Bösmann A, Preuster P, Wasserscheid P, Koller TM, Rausch MH, Fröba AP. Effect of the degree of hydrogenation on the viscosity, surface tension, and density of the liquid organic hydrogen carrier system based on diphenylmethane. Int J Hydrogen Energy 2022;47:6111–30. https://doi.org/10.1016/j.ijhydene.2021.11.198.
[15] Jander JH, Kerscher M, Cui J, Wicklein J, Rüde T, Preuster P, Rausch MH, Wasserscheid P, Koller TM, Fröba AP. Viscosity, surface tension, and density of the liquid organic hydrogen carrier system based on diphenylmethane, biphenyl, and benzophenone. Int J Hydrogen Energy 2022;47:22078–92. https://doi.org/10.1016/j.ijhydene.2022.04.275.
[16] Cui J, Kerscher M, Jander JH, Rüde T, Schulz PS, Wasserscheid P, Rausch MH, Koller TM, Fröba AP. Viscosity and surface tension of fluorene and perhydrofluorene close to 0.1 MPa up to 573 K. J Chem Eng Data 2022;67: 3085–96. https://doi.org/10.1021/acs.jced.2c00519.
[17] Kerscher M, Jander JH, Cui J, Martin MM, Wolf M, Preuster P, Rausch MH, Wasserscheid P, Koller TM, Fröba AP. Viscosity, surface tension, and density of binary mixtures of the liquid organic hydrogen carrier diphenylmethane with benzophenone. Int J Hydrogen Energy 2022;47:15789–806. https://doi.org/10.1016/j.ijhydene.2022.03.051.
[18] Jander JH, Schmidt PS, Giraudet C, Wasserscheid P, Rausch MH, Fröba AP. Hydrogen solubility, interfacial tension, and density of the liquid organic hydrogen carrier system diphenylmethane/dicyclohexylmethane. Int J Hydrogen Energy 2021;46:19446–66. https://doi.org/10.1016/j.ijhydene.2021.03.093.
[19] Kerscher M, Klein T, Preuster P, Wasserscheid P, Koller TM, Rausch MH, Fröba AP. Influence of dissolved hydrogen on the viscosity and interfacial tension of the liquid organic hydrogen carrier system based on diphenylmethane by surface light scattering and molecular dynamics simulations. Int J Hydrogen Energy 2022;47: 39163–78. https://doi.org/10.1016/j.ijhydene.2022.09.078.
[20] Aslam R, Müller K, Müller M, Koch M, Wasserscheid P, Arlt W. Measurement of hydrogen solubility in potential liquid organic hydrogen carriers. J Chem Eng Data 2016;61:643–9. https://doi.org/10.1021/acs.jced.5b00789.
[21] Qin X, Duan Q, Wang Y, Cui J, Zhang K, Bi S. Solubilities of hydrogen, nitrogen, and carbon dioxide in diphenylmethane. Fluid Phase Equil 2024;580:114055. https://doi.org/10.1016/j.fluid.2024.114055.
[22] Simnick JJ, Liu KD, Lin HM, Chao KC. Gas-liquid equilibrium in mixtures of hydrogen and diphenylmethane. Ind Eng Chem Process Des Dev 1978;17:204–8. https://doi.org/10.1021/i260066a015.
[23] Ziparo C, Giannasi A, Ulivi L, Zoppi M. Raman spectroscopy study of molecular hydrogen solubility in water at high pressure. Int J Hydrogen Energy 2011;36: 7951–5. https://doi.org/10.1016/j.ijhydene.2011.01.178.
[24] Kerscher M, Jander JH, Luther F, Schühle P, Richter M, Rausch MH, Fröba AP. Thermophysical properties of the energy carrier methanol under the influence of dissolved hydrogen. Int J Hydrogen Energy 2023;48:26817–39. https://doi.org/10.1016/j.ijhydene.2023.03.312.
[25] Kerscher M, Jander JH, Cui J, Maurer LA, Wolf P, Hofmann JD, Köksal A, Zachskorn H, Auer F, Schulz PS, Wasserscheid P, Rausch MH, Koller TM, Fröba AP. Thermophysical properties of the liquid organic hydrogen carrier system based on benzyltoluene considering influences of isomerism and dissolved hydrogen. Submitted to Int J Hydrog Energy 2024.
[26] May EF, Tay WJ, Nania M, Aleji A, Al-Ghafri S, Martin Trusler JP. Physical apparatus parameters and model for vibrating tube densimeters at pressures to 140 MPa and temperatures to 473 K. Rev Sci Instrum 2014;85. https://doi.org/10.1063/1.4894469.
[27] Leachman JW, Jacobsen RT, Penoncello SG, Lemmon EW. Fundamental equations of state for parahydrogen, normal hydrogen, and orthohydrogen. J Phys Chem Ref Data 2009;38:721–48. https://doi.org/10.1063/1.3160306.
[28] Lemmon EW, Bell IHMLH, McLinden MO. NIST standard reference database 23: reference fluid thermodynamic and transport properties-REFPROP. National Institute of Standards and Technology; 2018. https://doi.org/10.18434/T4/1502528. Version 10.0.
[29] Jorschick H, Geißelbrecht M, Eßl M, Preuster P, Bösmann A, Wasserscheid P. Benzyltoluene/dibenzyltoluene-based mixtures as suitable liquid organic hydrogen carrier systems for low temperature applications. Int J Hydrogen Energy 2020;45: 14897–906. https://doi.org/10.1016/j.ijhydene.2020.03.210.
[30] Grosse AV, Mavity JM, Mattox WJ. Catalytic dehydrogenation of polycyclic naphthenes. Ind Eng Chem 1946;38:1041–5. https://doi.org/10.1021/ie50442a019.
[31] Smith HA, Alderman DM, Shacklett CD, Welch CM. The catalytic hydrogenation of the benzene nucleus. VI. The hydrogenation of compounds with two benzene rings. J Am Chem Soc 1949;71:3772–6. https://doi.org/10.1021/ja01179a056.
[32] Serijan KT, Wise PH. Dicyclic hydrocarbons. III. Diphenyl- and dicyclohexylalkanes through C_{15}. J Am Chem Soc 1951;73:4766–9. https://doi.org/10.1021/ja01154a086.
[33] Jander JH, Piszko M, Kühl JVW, Rausch MH, Fröba AP. Solubility and liquid density of binary mixtures of *n*-hexane or 1-hexanol with krypton, sulfur hexafluoride, or R143a. J Chem Eng Data 2023;68:813–34. https://doi.org/10.1021/acs.jced.2c00727.
[34] Le Ru EC, Schroeter LC, Etchegoin PG. Direct measurement of resonance Raman spectra and cross sections by a polarization difference technique. Anal Chem 2012; 84:5074–9. https://doi.org/10.1021/ac300763q.
[35] Auguié B, Reigue A, Le Ru EC, Etchegoin PG. Tiny peaks vs mega backgrounds: a general spectroscopic method with applications in resonant Raman scattering and atmospheric absorptions. Anal Chem 2012;84:7938–45. https://doi.org/10.1021/ac301696p.
[36] Hase H, Ishioka K, Miyatake Y, Kobayashi M, Kobayashi M. Raman study of ethanol and ethanolic solutions of LiCl at low temperatures. J Phys Chem 1991;95:8541–6. https://doi.org/10.1021/j100175a025.
[37] Singh DK, Mishra S, Ojha AK, Srivastava SK, Schlücker S, Asthana BP, Popp J, Singh RK. Hydrogen bonding in different pyrimidine-methanol clusters probed by polarized Raman spectroscopy and DFT calculations. J Raman Spectrosc 2011;42: 667–75. https://doi.org/10.1002/jrs.2744.
[38] Dracopoulos V, Papatheodorou GN. Isotropic and anisotropic Raman scattering from molten alkali-metal fluorides. Phys Chem Chem Phys 2000;2:2021–5. https://doi.org/10.1039/b000803f.
[39] Hrovat Mirko. Baseline fit (version januar 2009). https://de.mathworks.com/matlabcentral/fileexchange/24916-baseline-fit?focused=5133659&tab=function; 2009.
[40] Luther SK, Schuster JJ, Leipertz A, Braeuer A. Non-invasive quantification of phase equilibria of ternary mixtures composed of carbon dioxide, organic solvent and water. J Supercrit Fluids 2013;84:146–54. https://doi.org/10.1016/j.supflu.2013.09.012.
[41] Cukor PM, Prausnitz JM. Solubilities of gases in liquids at elevated temperatures. Henry's constants for hydrogen, methane, and ethane in hexadecane, bicyclohexyl, and diphenylmethane. J Phys Chem 1972;76:598–601. https://doi.org/10.1021/j100648a026.
[42] Hefter GT, Tomkins RPT. The experimental determination of solubilities. John Wiley & Sons; 2005. https://doi.org/10.1002/0470867833.
[43] Dymond J, Hildebrand JH. Apparatus for accurate, rapid determinations of solubility of gases in liquids. Ind Eng Chem Fundam 1967;6:130–1. https://doi.org/10.1021/i160021a022.
[44] Jander JH, Kerscher M, Li S, Rausch MH, Wasserscheid P, Fröba AP. Determination of hydrogen loading in the carrier system diphenylmethane/dicyclohexylmethane by depolarized Raman spectroscopy. Int J Hydrogen Energy 2022;47:9331–45. https://doi.org/10.1016/j.ijhydene.2022.01.005.
[45] Kerscher M, Klein T, Schulz PS, Veroutis E, Dürr S, Preuster P, Koller TM, Rausch MH, Economou IG, Wasserscheid P, Fröba AP. Thermophysical properties of diphenylmethane and dicyclohexylmethane as a reference liquid organic hydrogen carrier system from experiments and molecular simulations. Int J Hydrogen Energy 2020;45:28903–19. https://doi.org/10.1016/j.ijhydene.2020.07.261.